

Mn_{0.06}Ge_{0.94} diluted magnetic semiconductor epitaxially grown on Ge(001): Influence of Mn₅Ge₃ nanoscopic clusters on the electronic and magnetic properties

P. De Padova,¹ J.-P. Ayoub,² I. Berbezier,² P. Perfetti,¹ C. Quaresima,¹ A. M. Testa,¹ D. Fiorani,¹ B. Olivieri,³ J.-M. Mariot,⁴ A. Taleb-Ibrahimi,⁵ M. C. Richter,⁶ O. Heckmann,⁶ and K. Hricovini⁶

¹CNR, Istituto di Struttura della Materia, Via Fosso del Cavaliere, 00133 Roma, Italy

²Laboratoire Matériaux et Microélectronique de Provence (UMR 6137), Faculté des Sciences et Techniques, Campus de Saint Jérôme, Case 142, Avenue Normandie Niemen, 13397 Marseille Cedex 20, France

³CNR, Istituto di Scienze dell'Atmosfera e del Clima, Via Fosso del Cavaliere, 00133 Roma, Italy

⁴Laboratoire de Chimie Physique—Matière et Rayonnement (UMR 7614), Université Pierre et Marie Curie, 11 Rue Pierre et Marie Curie, 75231 Paris Cedex 05, France

⁵Synchrotron SOLEIL, L'Orme des Merisiers, Saint-Aubin, Boîte Postale 48, 91192 Gif-sur-Yvette Cedex, France

⁶Laboratoire de Physique des Matériaux et des Surfaces, Université de Cergy-Pontoise, 5 Mail Gay-Lussac, 95031 Cergy-Pontoise, France

(Received 11 July 2007; revised manuscript received 21 September 2007; published 8 January 2008)

The structural, electronic, and magnetic properties of the Mn_{0.06}Ge_{0.94} diluted magnetic semiconductor, grown at 520 K by molecular-beam epitaxy on Ge(001)2×1, have been investigated. Diluted and highly ordered alloys, containing Mn₅Ge₃ nanocrystals, were grown. The valence band photoelectron spectrum of Mn_{0.06}Ge_{0.94} shows a feature located at -4.2 eV below the Fermi level, which is the fingerprint of substitutional Mn atoms in the Ge matrix. Magnetization measurements show the presence of a paramagnetic component due to substitutional Mn atoms and of a ferromagneticlike component due to Mn₅Ge₃ nanocrystallites. The Mn *L*_{2,3} x-ray absorption spectrum of this polyphase film shows no marked multiplet structure, but a bandlike character.

DOI: [10.1103/PhysRevB.77.045203](https://doi.org/10.1103/PhysRevB.77.045203)

PACS number(s): 75.50.Pp, 79.60.-i, 78.70.Dm, 75.70.-i

I. INTRODUCTION

Diluted magnetic semiconductors (DMSs) are a class of materials where magnetic atoms are added to nonmagnetic semiconductors.^{1,2} They are currently the object of intense research for spintronic applications. In particular, Mn-doped germanium is an attractive system because of its high Curie temperature (T_C) (see Refs. 2 and 3) and its compatibility with the Si-based technology.

Due to the high reactivity between Mn and Ge, several ferromagnetic (FM) precipitates, such as Mn₁₁Ge₈, Mn₃Ge₂, and Mn₅Ge₃,⁴⁻⁷ can appear during the growth of Mn_xGe_{1-x}, substrate temperature, growth rate, and Mn concentration being the main ingredients determining the properties of Mn-doped germanium.^{3,4,8,9} A separation between Mn-rich and Mn-depleted phases was found in Mn_{0.06}Ge_{0.94} single crystals,⁴ as well as in Mn_xGe_{1-x} alloys prepared by ion implantation,¹⁰ and in Mn_xGe_{1-x} films grown by molecular-beam epitaxy (MBE) at high temperature (≈ 520 K).^{9,11,12} The role played by the Mn₅Ge₃ secondary phase in determining the FM properties at high temperature of Mn_xGe_{1-x} films has also been discussed.⁹⁻¹³

Very recently, a new phase with composition close to Ge₂Mn, i.e., corresponding to an unknown Ge-rich phase, has been reported by Jamet *et al.*¹⁴ during the epitaxial growth of Mn_{0.06}Ge_{0.94} films. These authors found that the Mn distribution was strongly inhomogeneous. They observed the eutectoid growth of well-defined Mn-rich (Ge₂Mn) nanocolumns surrounded by a Mn-poor matrix, the large magnetization at high temperature of their samples being consistent with a T_C greater than 400 K. Magnetotransport revealed a large anomalous Hall effect up to room temperature, while a

giant positive magnetoresistance (MR) was measured with no evidence of saturation. After this work, Li *et al.*¹⁵ observed similar nanocolumns, although their composition, structure, and spatial distribution were slightly different. They found on Mn_{0.05}Ge_{0.95} DMSs grown at 353 K a giant positive MR directly correlated with the distribution of Mn magnetic impurities. Postannealing at 473 K increases Mn substitution in the host matrix above the threshold for insulator-metal transition, maintaining the columnar morphology and having a global ferromagnetism with conventional negative MR. Li *et al.*¹⁵ did not observe either a T_C greater than 400 K or the giant orbital MR found by Jamet *et al.*¹⁴ This reinforces the idea that the magnetic and transport properties of these systems are highly sensitive to the dopant location and distribution.

Park *et al.*³ and Li *et al.*⁸ reported magnetization measurements as a function of temperature, respectively, for ≈ 60 nm thick Mn_{0.02}Ge_{0.98} and 70 nm thick Mn_{0.05}Ge_{0.95} films, grown at 353 K. The magnetic behavior in both samples shows similarities, i.e., a kink near 110 K attributed in the first case to a long-range magnetic transition based on hole-mediated spin exchange interactions and in the second case to a short-range magnetic transition inside spin clusters associated with inhomogeneities in the Mn distribution. Li *et al.*⁸ also observed hysteresis loops at 5 K in their sample, but no remanence between 20 and 110 K, the transition temperature between the two regimes being 12 K. These authors concluded for the presence of two magnetic transitions in the samples: one at $T_C \approx 12$ K, which corresponds to the FM ordering temperature for Mn_xGe_{1-x} DMS, and another at $T_C^* \approx 110$ K related to a FM ordering within spin clusters.

Being element specific, x-ray absorption spectroscopy (XAS) is a useful tool to understand the electronic structure of the magnetic atom in the semiconducting host. However, in spite of extensive works,^{4,16–19} there is no consensus as concerns the line shape of the Mn $L_{2,3}$ XAS spectrum in DMSs. For instance, in $(\text{Ga}_{1-x}\text{Mn}_x)\text{As}$ and $\text{Mn}_x\text{Ge}_{1-x}$ DMSs,^{17,18} the rich multiplet structure, similar to that observed in MnO (see, e.g., Ref. 20), has been attributed to the localized $3d$ states of Mn^{2+} ions in substitutional sites of the host lattice. However, it has been shown recently for $(\text{Ga}_{1-x}\text{Mn}_x)\text{As}$ and $\text{Mn}_{0.025}\text{Ge}_{0.975}$ DMSs that this multiplet structure corresponds to Mn oxide^{16,22} or to nonmagnetic Mn atoms on the surface.²³

In this paper, we report a detailed structural and electronic and magnetic study of $\text{Mn}_x\text{Ge}_{1-x}$ and Mn_5Ge_3 films, grown by MBE on Ge(001) and Ge(111), respectively, using high-resolution transmission electron microscopy (HRTEM), selected-area electron diffraction (SAED), photoelectron spectroscopy (PES), XAS and x-ray magnetic circular dichroism (XMCD) at the Mn $L_{2,3}$ edge, and superconducting quantum interference device (SQUID) magnetometry. We have previously reported preliminary results on the structural and electronic and magnetic properties of such films in which substitutional Mn atoms included into Ge matrix and nanoscopic Mn_5Ge_3 crystallites with a mean size of 3 nm are clearly identified in the $\text{Mn}_x\text{Ge}_{1-x}$ films.^{11,13,21} Here, in the light of spectroscopic data, we give a unified account of our results concerning (1) the electronic properties of both $\text{Mn}_{0.06}\text{Ge}_{0.94}$ DMS and Mn_5Ge_3 samples, as observed from valence band (VB) PES, which clearly demonstrates in $\text{Mn}_{0.06}\text{Ge}_{0.94}$ DMS the coexistence of Mn inclusions in the Ge lattice and the formation of Mn_5Ge_3 alloy clusters; (2) the comparison of the magnetic behavior between $\text{Mn}_{0.06}\text{Ge}_{0.94}$ containing Mn_5Ge_3 nanoclusters and $\text{Mn}_{0.03}\text{Ge}_{0.97}$ free from such nanoclusters; (3) the two-dimensional XY behavior of the Mn_5Ge_3 thin films; and (4) the role played by oxygen contamination in defining the XAS/XMCD spectra of the $\text{Mn}_x\text{Ge}_{1-x}$ films.

II. EXPERIMENT

PES and XAS measurements were carried out in an ultra-high vacuum (UHV) chamber (base pressure of 3×10^{-10} mbar) using synchrotron radiation on the D1011 beamline at MAX-lab (Lund, Sweden) on samples prepared *in situ* under a pressure not exceeding 5×10^{-10} mbar by MBE on Ge(001) 2×1 substrates held at 520 K, conditions known to favor both the epitaxial growth of DMS, and the formation of FM clusters.^{8,9,11} The same samples were used later for the HRTEM, SAED, and SQUID measurements. Mn_5Ge_3 films were also prepared by solid-state epitaxy⁷ by depositing a few monolayers (ML) of manganese on Ge(111)-c(8×2) and subsequent annealing at 730 K for 15 min. The epitaxy between the [0001] and [111] planes of the film and the Ge substrate was evidenced by reflection high-energy electron diffraction (RHEED) patterns, which showed sharp $(\sqrt{3} \times \sqrt{3})R30^\circ$ streaks with incident beam along the $[11\bar{2}]$ direction. This is in agreement with the for-

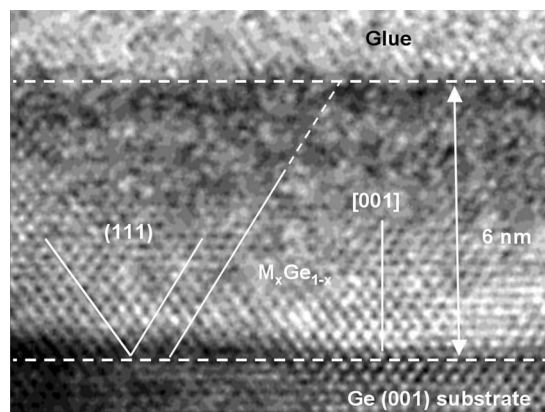


FIG. 1. Cross-sectional HRTEM image of a $\text{Mn}_{0.06}\text{Ge}_{0.94}$ film grown on a Ge(001) 2×1 substrate held at 520 K.

mation of Mn_5Ge_3 single crystals with a $D8_g$ -type structure.⁷ The PES spectra were obtained with a total instrumental resolution of 50 meV using a Scienta SES200 electron energy analyzer in integrated mode. The Mn $L_{2,3}$ XAS spectra were recorded in the total electron yield mode, with a total energy resolution of 0.2 eV. XMCD measurements were done in remanence on samples held at $T \approx 80$ K and having been submitted to an ≈ 1 kOe magnetic field.

III. RESULTS AND DISCUSSION

A. Growth

A cross-sectional HRTEM image of a 6 nm thick $\text{Mn}_{0.06}\text{Ge}_{0.94}$ film, collected with a 200 keV beam along the [110] direction, is shown in Fig. 1. The film is of perfect crystallinity, as demonstrated by the alignment of the (111) planes in the substrate and the film and by the absence of impurities and crystalline defects at the interface, along (on average) several hundreds of nanometers. In the epitaxial region, which extends up to the surface, no contrast is induced by the dilution of Mn in the Ge matrix, which suggests that Mn atoms are mainly located in substitutional sites. SAED provides further information on the film structure near the interface.¹¹ A detailed analysis of the diffraction spots shows the superposition of two lattices (Ge and Mn:Ge), indicating a small difference between the lattice parameters of the film near the interface and those of the substrate. This can be attributed to the mismatch between the atomic volumes of Mn and Ge.

The almost continuous film is interrupted by randomly distributed 3 nm nanocrystalline Mn_5Ge_3 secondary phase precipitates, as identified by SAED. Precipitates with other Mn concentrations have not been detected. By studying the size of the Mn_5Ge_3 precipitates on several $\text{Mn}_x\text{Ge}_{1-x}$ samples ($0.005 < x < 0.10$; $6 \text{ nm} < \text{thickness} < 85 \text{ nm}$) grown on Ge(001) at 520 K, a 1.5%–2% Mn concentration has been deduced. This value agrees with that (2%) reported from spatially resolved energy-dispersive x-ray spectroscopy measurements.^{9,12,14} The size and structural ordering of these precipitates are found to increase with Mn concentration and film thickness. All the samples show a part of epitaxial film

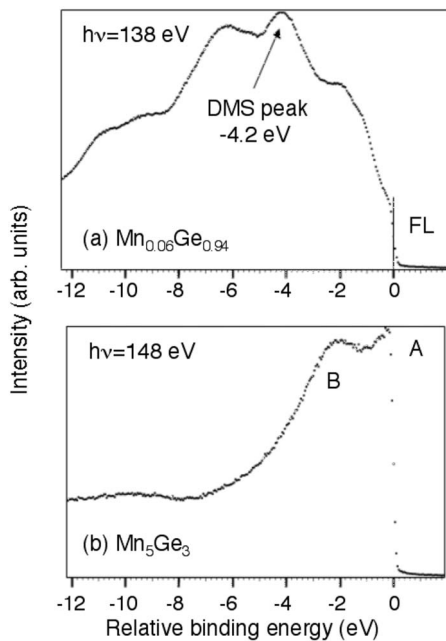


FIG. 2. VB PES spectra of (a) Mn_{0.06}Ge_{0.94} and (b) Mn₅Ge₃ films.

free from precipitates, while the remaining part contains Mn₅Ge₃ inclusions.¹¹ On the basis of these findings, we conclude that the lattice strain associated with the Mn atoms in substitutional sites controls and limits the growth of the diluted alloys. The Mn_xGe_{1-x} lattice swells up to a critical strain above which Mn atoms segregate in Mn-rich nanocrystals. A similar mechanism has been observed in the (Ga_{1-x}Mn_x)As DMS.¹⁶

B. Photoemission

The presence of Mn_xGe_{1-x} DMS at the surface of the sample is further demonstrated by PES. Figure 2 shows the VB spectra of Mn_{0.06}Ge_{0.94} and Mn₅Ge₃ films recorded after growth at photon energies $h\nu=138$ and 148 eV, respectively. The VB spectra were collected immediately after the film growth in order to prevent surface contamination. The absence of the O(1s) peak was carefully checked. There are two important signatures in the spectrum. First, we emphasize the presence of a peak at about -4.2 eV binding energy (BE) in the VB spectrum of Mn_{0.06}Ge_{0.94} [Fig. 2(a)]. This structure is very similar to that observed in Ga_{0.069}Mn_{0.939}As (Ref. 24) and Mn_{0.06}Ge_{0.94} (Ref. 4) and is attributed to Mn 3d states hybridized with the band states of the semiconductor host. Second, there is a weak electron emission at the Fermi level (FL), evidencing the presence of a metallic component in the Mn_xGe_{1-x} alloy. This VB PES spectrum is of major importance because it demonstrates the coexistence of diluted Mn atoms in the Ge matrix with Mn₅Ge₃ clusters, in agreement with the HRTEM measurements. Note that recent calculations¹⁰ suggest that the peak at -4.2 eV in the VB is a fingerprint of substitutional Mn atoms in a Ge matrix. The VB spectrum of Mn₅Ge₃ [Fig. 2(b)] shows a clear cutoff at the FL, as expected from its metallic behavior.²⁵ Two fea-

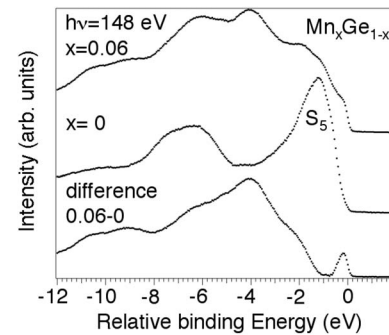


FIG. 3. VB PES spectra of Mn_xGe_{1-x} for $x=0.06$ and $x=0$ (clean Ge substrate). The difference spectrum is given at the bottom of the figure.

tures are observed: one (A) at the FL and the other (B) at ≈ -2 eV BE. They are characteristic of the Mn 3d density of states (DOS) in Mn₅Ge₃.^{25,26}

In order to give a qualitative insight of Mn 3d DOS, we show in Fig. 3 the difference between the VB PES spectra of Mn_{0.06}Ge_{0.94} and of a clean Ge(001) 2×1 surface. The difference spectrum exhibits the two structures discussed above. Now, the contribution of the Mn₅Ge₃ clusters is more clearly seen in the vicinity of the FL. The contribution of the Mn 3d DOS in Mn₅Ge₃ appears also as a shoulder at -2 eV BE.

C. Mn L_{2,3} x-ray absorption

The Mn L_{2,3} XAS spectra allow us to obtain further information on the Mn electronic structure in the films. Despite the UHV conditions used (see Sec. II), the Mn_{0.06}Ge_{0.94} samples, clean after growth, result in a partially oxidized surface during the XAS data acquisition (a few hours). So to prevent surface oxidation and to study the Mn L_{2,3} XAS spectrum of a clean Mn_{0.06}Ge_{0.94} alloy, the *in situ* grown samples were capped with ≈ 2 ML of germanium.

Figure 4 shows the Mn L₃ XAS spectra of an uncapped Mn_{0.06}Ge_{0.94} film, of a capped Mn_{0.06}Ge_{0.94} film, and of a Mn₅Ge₃ film.

When compared to the XAS spectrum of the uncapped sample, the XAS spectrum of the capped sample exhibits a broad line shape with a reduced fine structure, similar to that of the Mn₅Ge₃ spectrum. This reflects the hybridization between the Mn 3d states and the Ge 4s4p valence states, i.e., a marked delocalization of the Mn 3d states. The spectrum of the uncapped alloy has a more pronounced multiplet structure, strongly enhanced when the surface sample is exposed to air (spectrum not reported), corresponding to Mn atoms in the d^5 high-spin state characteristic of MnO (see, for instance, Ref. 20). The difference in surface contamination between the capped and uncapped samples is confirmed by PES measurements: In the uncapped sample, the O(1s) spectrum splits into two components attributed to the GeO- and MnO-like oxides, whereas only the GeO-like oxide, corresponding to the contamination of the capping Ge layer, is found on the capped film, which is now free of oxidized Mn atoms.²¹ This result may appear at variance with a number of previous XAS results.^{4,17,18} However, they are in line with

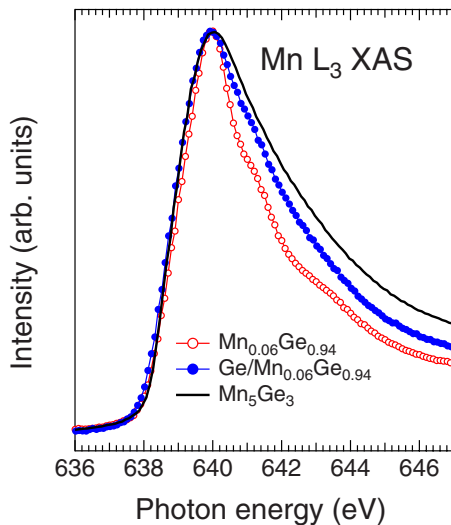


FIG. 4. (Color online) Comparison between the shapes of the Mn L_3 XAS spectra of an uncapped $\text{Mn}_{0.06}\text{Ge}_{0.94}$ film (6 nm), of a Ge-capped $\text{Mn}_{0.06}\text{Ge}_{0.94}$ film (6 nm), and of a Mn_5Ge_3 film (25 nm).

recent findings for etched $(\text{Ga}_{1-x}\text{Mn}_x)\text{As}$, $\text{Mn}_x\text{Ge}_{1-x}$ films, and Mn impurities deposited on Ge and GaAs surfaces.^{16,19,22} One should also note the absence in the L_3 white line of the prepeak expected from first-principles calculations to appear when interstitial Mn atoms are present in the Ge lattice.¹⁸ This can be considered as a confirmation that the Mn atoms diluted in the Ge host are substitutional. It is also interesting to note that a broadening of the multiplet structure due to the partial delocalization of the Mn $3d$ states is observed for diluted Mn impurities on a Ge surface, where the degree of hybridization with Ge $4s4p$ states is presumably reduced in comparison to the bulk impurity configuration.^{19,22}

The XAS shape of the capped sample, even showing a reduced multiplet structure with respect to the uncapped film, is rather different from that of pure Mn_5Ge_3 . The XAS line shape we observe for the $\text{Mn}_x\text{Ge}_{1-x}$ film should consist of the contributions arising from substitutional Mn diluted in the Ge host and from Mn included in the Mn_5Ge_3 nanocrystallites. Although it is difficult to estimate quantitatively the proportion between these two spectral components and to attempt a decomposition, one can resort to simple arguments to discuss their main qualitative features. HRTEM analysis and magnetic results (see below) show that the diluted sample strongly contributes to the whole film. Then, the differences in shape and in width of the XAS spectra of clean $\text{Mn}_{0.06}\text{Ge}_{0.94}$ and Mn_5Ge_3 films reveal differences in the Mn hybridization states in these samples, confirming the presence of Mn atoms in the Ge matrix with an environment different from those encountered in Mn_5Ge_3 . This result is in agreement with the VB PES spectrum of $\text{Mn}_{0.06}\text{Ge}_{0.94}$ reported in Fig. 2(a), which is determined by the electronic DOS of both the diluted $\text{Mn}_x\text{Ge}_{1-x}$ and the Mn_5Ge_3 alloys.

D. Magnetic properties

In order to correlate the structural and electronic structure information with the magnetic properties, the films were in-

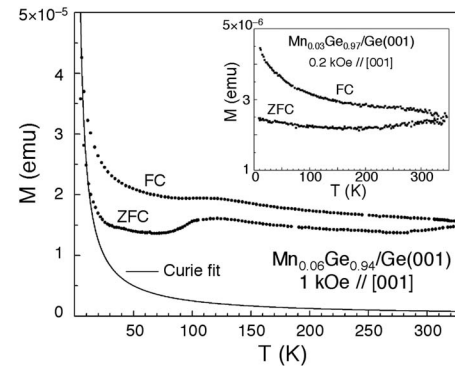


FIG. 5. Zero-field-cooled and field-cooled temperature dependence of the magnetization for a $\text{Mn}_{0.06}\text{Ge}_{0.94}$ film measured with a magnetic field $H=1$ kOe parallel to the surface of the film ([001] direction). The solid line is the Curie fit to the low temperature part of the ZFC curve. The inset shows the corresponding curves for a 6 nm thick $\text{Mn}_{0.03}\text{Ge}_{0.97}$ sample prepared at low temperature (353 K), which is free from Mn_5Ge_3 precipitates.

vestigated by SQUID magnetometry. Magnetization has been recorded as a function of temperature ($5 \text{ K} \leq T \leq 330 \text{ K}$) and magnetic field (up to 20 kOe) applied parallel to the surface of the film ([001] direction). Figure 5 shows the temperature dependence of the magnetization M for a $\text{Mn}_{0.06}\text{Ge}_{0.94}$ film. A magnetic field of 1 kOe was applied parallel to the film plane. The magnetization was measured (see Fig. 5) for increasing temperature after zero-field cooling (ZFC) and then for decreasing temperature at the same magnetic field [field cooling (FC) process]. The ZFC curve shows three main features associated with different types of contributions to the magnetization: (i) First is a low temperature Curie-like behavior, revealing the presence of paramagnetic (PM) entities, as confirmed by the Curie fit; this contribution is attributed to the substitutional Mn atoms in the Ge host. (ii) Second is a broad maximum at higher temperature, characteristic of a blocking process of moments of magnetic nanoparticles with a large size distribution; this contribution is associated with FM Mn_5Ge_3 precipitates ($T_C \approx 310 \text{ K}$ in the bulk²⁷) of different sizes (identified by SAED) having moments that block progressively with decreasing temperature, giving rise to the observed irreversibility (difference between FC and ZFC). Note that this bump is not observed (see the inset to Fig. 5) in the ZFC curve characteristic of 6 nm $\text{Mn}_{0.03}\text{Ge}_{0.97}$ films prepared at low temperature (353 K), i.e., in which Mn_5Ge_3 precipitates are absent. (iii) Third is a small increase of magnetization above 290 K, indicating the tendency toward a second broad maximum, probably due either to bigger FM precipitates or to the Ge_2Mn -like phase ($T_C > 400 \text{ K}$) recently discovered by Jamet *et al.*,¹⁴ too diluted to be detected by SAED. Such a Mn-rich phase could explain (see inset to Fig. 5) the weak increase in the ZFC magnetization observed above $\approx 200 \text{ K}$ in $\text{Mn}_{0.03}\text{Ge}_{0.97}$, as well as the downward curvature observed in the FC magnetization above $\approx 250 \text{ K}$. These results are coherent with the irreversibility observed over the whole temperature range, confirming the occurrence of moment blocking processes below 330 K (the highest measuring temperature) and with the results of the $M(H)$

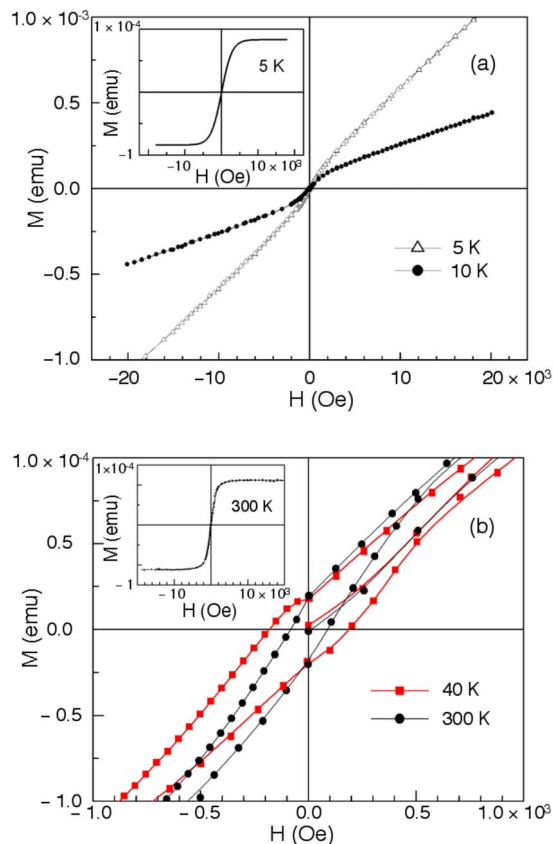


FIG. 6. (Color online) $M(H)$ loops of a $\text{Mn}_{0.06}\text{Ge}_{0.94}$ film: (a) Loops at 5 and 10 K with $-20 \text{ kOe} < H < +20 \text{ kOe}$. The curve given as an inset is obtained by subtracting a linear curve to the $M(H)$ behavior measured at 5 K. (b) Loops at 40 and 300 K with $-1 \text{ kOe} < H < +1 \text{ kOe}$. The inset is the $M(H)$ loop at 300 K with $-20 \text{ kOe} < H < +20 \text{ kOe}$.

measurements shown in Fig. 6. On the other hand, there is no evidence of a clear T_C for Mn_5Ge_3 , probably because the large size distribution of the precipitates determines a T_C distribution. Indeed, the low temperature measurements [Fig. 6(a)] show the coexistence of a saturating FM-like component giving rise to a small bump at low fields, due to the blocked moments of the Mn_5Ge_3 precipitates, and a nonsaturating PM component responsible for the linear variation at higher field. This is more clearly observable at 10 K. The FM contribution is better evidenced when the linear PM contribution is subtracted from the $M(H)$ curve [Fig. 6(a), inset]. The FM contribution is more evident at higher temperature because of the decrease of the PM contribution. Indeed, the magnetization curves at 40 and 300 K given in Fig. 6(b) show a clear hysteretic behavior. The presence of a coercive field even at 300 K ($H_c = 100 \text{ Oe}$), well above the temperature range of the broad maximum in the $M(T)$ curve, is coherent with the small increase of M observed above 290 K.

Figure 7 displays the reduced magnetization $R = M(T)/M(50 \text{ K})$ (50 K) as a function of T of a Mn_5Ge_3 film. $M(H)$ hysteresis loops at $20 \text{ K} < T < 300 \text{ K}$ show (the loop at 300 K is given in the left inset) typical features of FM ordering, with a coercive field of 300 Oe and a transition temperature $T_C = 303 \text{ K}$ deduced from the peak temperature of dM/dT (right

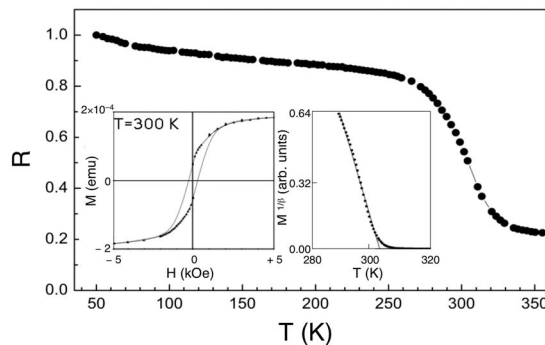


FIG. 7. Reduced magnetization $R = M(T)/M(50 \text{ K})$ as a function of temperature ($H_a = 200 \text{ Oe}$) for $\text{Mn}_5\text{Ge}_3/\text{Ge}(111)\text{-}c(8 \times 2)$. Insets: $M(H)$ loop at 300 K (left); $(1 - T/T_C)^\beta$ fit of the $M(T)$ curve near T_C (right).

inset), close to that ($\approx 310 \text{ K}$) of bulk Mn_5Ge_3 .²⁷ Our value of T_C is slightly higher than that reported recently⁷ in similar samples ($T_C = 296 \text{ K}$). We suggest that the Curie temperature of Mn_5Ge_3 films is strongly dependent on the quality and stoichiometry of the sample. From the measured value of the magnetic moment at saturation and taking into account the thickness of the film (30 nm), an atomic magnetic moment $m_s = (2.26 \pm 0.5)\mu_B$ is deduced, which is in good agreement with the values obtained from the XMCD measurements reported below and in Ref. 7. To have better insight into the nature of the magnetic phase transition, we fitted (solid line between the experimental points in Fig. 7) the magnetization in the vicinity of T_C to a $M(T) = M_0(1 - T/T_C)^\beta$ law, valid for the ferromagnets.²⁸ We obtain a critical exponent $\beta = 0.20 \pm 0.04$, in satisfactory agreement with the $(3\pi^2/128) \approx 0.231$ value, which is the universal signature of finite-sized two-dimensional XY behavior,²⁸ applicable to layered magnets for which the hysteresis loop exists only in the XY plane. This indicates that our sample is a single crystal, as also seen from the RHEED patterns.

Finally, the magnetic behavior of a Mn_5Ge_3 film was also studied by XMCD at the Mn $L_{2,3}$ absorption edge. Figure 8 shows the XAS spectrum recorded for parallel (I^+) and anti-parallel (I^-) alignments of the photon helicity with the magnetization. The XMCD signal ($I^+ - I^-$) is shown in the lower part of Fig. 8. The incidence angle of the photon beam was set to 45° to probe both in-plane and out-of-plane components of the sample magnetization. A remanent XMCD signal is observed at 80 K (see also Ref. 25). We applied the sum rules²⁹ to calculate the orbital and spin magnetic moments in Ge_3Mn_5 . It appears that the orbital moment contributes negligibly to the magnetism, in agreement with Ref. 30, and that the average total magnetic momentum per hole $m_{\text{tot}} = \langle L_z \rangle + 2\langle S_z \rangle$ is equal to $2.34\mu_B$. This is in good agreement with the average magnetic moment per Mn atom $m_s = (2.6 \pm 0.5)\mu_B$ measured by SQUID at 5 K. At variance, the flat XMCD signal obtained for $\text{Mn}_{0.06}\text{Ge}_{0.94}$ films shows the absence of magnetic remanence, confirming the PM behavior of Mn atoms substitutionally included in a Ge matrix at low concentration ($x \approx 1.5$).

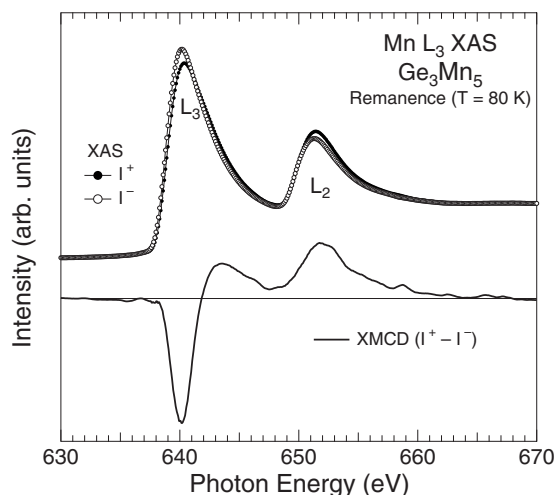


FIG. 8. Mn $L_{2,3}$ XAS spectra for a parallel (I^+) and an antiparallel (I^-) alignment of the photon helicity with the remanent magnetization and the corresponding XMCD signal in a Mn_5Ge_3 film.

IV. CONCLUSIONS

In conclusion, we prepared and investigated $Mn_{0.06}Ge_{0.94}$ single crystalline thin films. HRTEM and SAED measurements give evidence of the presence of Mn_5Ge_3 nanocrystalline precipitates inside a DMS film. The substitutional character of Mn atoms in the Ge host is shown from VB PES

spectra, which exhibit at -4.2 eV binding energy a feature characteristic of the Mn $3d$ states in a DMS, while these states are located at -2 eV in Mn_5Ge_3 . The Mn $L_{2,3}$ XAS spectrum of this polyphase sample presents a faint multiplet structure and is similar to that observed for Mn_5Ge_3 . The XAS line shape is very sensitive to the surface oxidation of the sample, upon which the multiplet structure is enhanced. The combination of microstructural and magnetic studies allowed us to identify the PM behavior of the Mn substitutional atoms (1.5%) in the Ge lattice sites and to show that the hysteretical behavior is due to the Mn_5Ge_3 nanoprecipitates dispersed in the Ge host. This magnetic behavior of the nanoprecipitates suggests that they can be used as a way to tune the magnetic properties for engineering spintronic devices.

ACKNOWLEDGMENTS

The authors thank the staff of the D1011 (MAX-lab) and VUV (ELETTRA) beamlines, and M. Capozzi and S. Priori for technical assistance. Support by the EU–Research Infrastructure Action under the FP6 “Structuring the European Research Area” Programme (through the Integrated Infrastructure Initiative “Integrating Activity on Synchrotron and Free Electron Laser Science”) and the Italian CNR/MIUR (FISR: “Nanotecnologie per dispositivi di memoria ad altissima densità”; FIRB: “Nanotecnologie e nanodispositivi, optoelettronici, elettronici e spintronici”) is also acknowledged.

- ¹S. A. Wolf, D. D. Awschalom, R. A. Buhrman, J. M. Daughton, S. von Molnár, M. L. Roukes, A. Y. Chtchelkanova, and D. M. Treger, *Science* **294**, 1488 (2001).
- ²T. Dietl, H. Ohno, F. Matsukura, J. Cibert, and D. Ferrand, *Science* **287**, 1019 (2000).
- ³Y. D. Park, A. T. Hanbicki, S. C. Erwin, C. S. Hellberg, J. M. Sullivan, J. E. Mattson, T. F. Ambrose, A. Wilson, G. Spanos, and B. T. Jonker, *Science* **295**, 651 (2002).
- ⁴J.-S. Kang, G. Kim, S. C. Wi, S. S. Lee, S. Choi, S. Cho, S. W. Han, K. H. Kim, H. J. Song, H. J. Shin, A. Sekiyama, S. Kasai, S. Suga, and B. I. Min, *Phys. Rev. Lett.* **94**, 147202 (2005).
- ⁵N. Yamada, K. Maeda, Y. Usami, and T. Ohoyama, *J. Phys. Soc. Jpn.* **55**, 3721 (1986).
- ⁶S. Cho, S. Choi, S. C. Hong, Y. Kim, J. B. Ketterson, B.-J. Kim, Y. C. Kim, and J.-H. Jung, *Phys. Rev. B* **66**, 033303 (2002).
- ⁷C. Zeng, S. C. Erwin, L. C. Feldman, A. P. Li, R. Jin, Y. Song, J. R. Thompson, and H. H. Weitering, *Appl. Phys. Lett.* **83**, 5002 (2003).
- ⁸A. P. Li, J. F. Wendelken, J. Shen, L. C. Feldman, J. R. Thompson, and H. H. Weitering, *Phys. Rev. B* **72**, 195205 (2005).
- ⁹C. Bihler, C. Jaeger, T. Vallaitis, M. Gjukic, M. S. Brandt, E. Pippel, J. Woltersdorf, and U. Gösele, *Appl. Phys. Lett.* **88**, 112506 (2006).
- ¹⁰L. Ottaviano, M. Passacantando, S. Picozzi, A. Continenza, R. Gunnella, A. Verna, G. Impellizzeri, and F. Priolo, *Appl. Phys. Lett.* **88**, 061907 (2006).
- ¹¹P. De Padova, L. Favre, I. Berbezier, B. Olivieri, A. Generosi, B. Paci, V. Rossi Albertini, P. Perfetti, C. Quaresima, J.-M. Mariot, A. Taleb-Ibrahimi, M. C. Richter, O. Heckmann, F. D’Orazio, F. Lucari, and K. Hricovini, *Surf. Sci.* **601**, 4370 (2007).
- ¹²L. Morresi, J.-P. Ayoub, N. Pinto, M. Ficcadenti, R. Murri, A. Ronda, and I. Berbezier, *Mater. Sci. Semicond. Process.* **9**, 836 (2006).
- ¹³J.-P. Ayoub, L. Favre, A. Ronda, I. Berbezier, P. De Padova, and B. Olivieri, *Mater. Sci. Semicond. Process.* **9**, 832 (2006).
- ¹⁴M. Jamet, A. Barski, T. Devillers, V. Poydenot, R. Dujardin, P. Bayle-Guillemaud, J. Rotheman, E. Bellet-Amalric, A. Marty, J. Cibert, R. Mattana, and S. Tatarenko, *Nat. Mater.* **5**, 653 (2006).
- ¹⁵A. P. Li, C. Zeng, K. van Benthem, M. F. Chisholm, J. Shen, S. V. S. Nageswara Rao, S. K. Dixit, L. C. Feldman, A. G. Petukhov, M. Foygel, and H. H. Weitering, *Phys. Rev. B* **75**, 201201(R) (2007).
- ¹⁶K. W. Edmonds, N. R. S. Fadley, R. P. Campion, C. T. Foxon, B. L. Gallagher, T. K. Johal, G. van der Laan, M. MacKenzie, J. N. Chapman, and E. Arenholz, *Appl. Phys. Lett.* **84**, 4065 (2004).
- ¹⁷H. Ohldag, V. Solinus, F. U. Hillebrecht, J. B. Goedkoop, M. Finazzi, F. Matsukura, and H. Ohno, *Appl. Phys. Lett.* **76**, 2928 (2000).
- ¹⁸S. Picozzi, L. Ottaviano, M. Passacantando, G. Profeta, A. Continenza, F. Priolo, M. Kim, and A. J. Freeman, *Appl. Phys. Lett.* **86**, 062501 (2005).
- ¹⁹P. Gambardella, H. Brune, S. S. Dhesi, P. Bencok, S. R. Krishna-

- kumar, S. Gardonio, M. Veronese, C. Grazioli, and C. Carbone, *Phys. Rev. B* **72**, 045337 (2005).
- ²⁰Y. Yonamoto, T. Yokoyama, K. Amemiya, D. Matsumura, and T. Ohta, *Phys. Rev. B* **63**, 214406 (2001).
- ²¹P. De Padova, J.-P. Ayoub, I. Berbezier, J.-M. Mariot, A. Taleb-Ibrahimi, M. C. Richter, O. Heckmann, A. M. Testa, D. Fiorani, B. Olivieri, S. Picozzi, and K. Hricovini, *Surf. Sci.* **601**, 2628 (2007).
- ²²P. Gambardella, L. Claude, S. Rusponi, K. J. Franke, H. Brune, J. Raabe, F. Nolting, P. Bencok, A. T. Hanbicki, B. T. Jonker, C. Grazioli, M. Veronese, and C. Carbone, *Phys. Rev. B* **75**, 125211 (2007).
- ²³D. Wu, D. J. Keavney, R. Wu, E. Johnston-Halperin, D. D. Awschalom, and J. Shi, *Phys. Rev. B* **71**, 153310 (2005).
- ²⁴J. Okabayashi, A. Kimura, T. Mizokawa, A. Fujimori, T. Hayashi, and M. Tanaka, *Phys. Rev. B* **59**, R2486 (1999).
- ²⁵C. Zeng, W. Zhu, S. C. Erwin, Z. Zhang, and H. H. Weitering, *Phys. Rev. B* **70**, 205340 (2004).
- ²⁶L. Sangaletti, E. Magnano, F. Bondino, C. Cepek, A. Sepe, and A. Goldoni, *Phys. Rev. B* **75**, 153311 (2007).
- ²⁷E. Sawatzky, *J. Appl. Phys.* **42**, 1706 (1971).
- ²⁸S. T. Bramwell and P. C. Holdsworth, *J. Phys.: Condens. Matter* **5**, L53 (1993).
- ²⁹B. T. Thole, P. Carra, F. Sette, and G. van der Laan, *Phys. Rev. Lett.* **68**, 1943 (1992).
- ³⁰C. Hirai, H. Sato, A. Kimura, K. Yaji, K. Iori, M. Taniguchi, K. Hiraoka, T. Muro, and A. Tanaka, *Physica B* **351**, 341 (2004).